



HAL
open science

Loading linear arrays of Cu(II) inside aromatic amide helices

Jinhua Wang, Barbara Wicher, Alejandro Mendez-Ardoy, Xuesong Li, Gilles Pecastaings, Thierry Buffeteau, Dario M. Bassani, Victor Maurizot, Ivan Huc

► **To cite this version:**

Jinhua Wang, Barbara Wicher, Alejandro Mendez-Ardoy, Xuesong Li, Gilles Pecastaings, et al.. Loading linear arrays of Cu(II) inside aromatic amide helices. *Angewandte Chemie International Edition*, 2021, 60 (34), pp.18461-18466. <10.1002/anie.202104734>. <hal-03281847>

HAL Id: hal-03281847

<https://hal.science/hal-03281847v1>

Submitted on 8 Jul 2021

HAL is a multi-disciplinary open access archive for the deposit and dissemination of scientific research documents, whether they are published or not. The documents may come from teaching and research institutions in France or abroad, or from public or private research centers.

L'archive ouverte pluridisciplinaire HAL, est destinée au dépôt et à la diffusion de documents scientifiques de niveau recherche, publiés ou non, émanant des établissements d'enseignement et de recherche français ou étrangers, des laboratoires publics ou privés.



Distributed under a Creative Commons CC BY-NC 4.0 - Attribution - Non-commercial use - International License

open up multiple opportunities for designing and fine-tuning new metallofoldamers.^[9]

Q_n oligomers combine several desirable properties, including remarkably stable conformations in a variety of solvents^[10] and rapid synthetic access.^[11] These organic helices have been shown to be effective multidimensional charge transporters along their axis,^[12] a property that may find applications in sensing.^[13] Holes are transported via a hopping mechanism both through covalent bonds along the helix and through space, that is, between aromatic layers stacked within the helix. The coexistence of alternative pathways may mitigate the effect of localized traps or defects. This results in a very small attenuation of charge transport with increasing helix length ($\beta = 0.06 \text{ \AA}^{-1}$) and high calculated hole mobilities of $0.1\text{--}1.0 \text{ cm}^2 \text{ V}^{-1} \text{ S}^{-1}$ along the helix axis.^[12a] In monolayers of Q_n oligomers on Au, charge transport perpendicular to the helix axis, that is, between helices, was found to be negligible even when helices are tightly packed. This evidences one-dimensional charge transport in contrast to other electroactive self-assembled monolayers.^[14]

Quinoline has been extensively used as a ligand to form complexes with various transition metal ions.^[4] We thus devised that metal ions might be coordinated by Q_n organic strands at the quinoline nitrogen atoms and, possibly, through amide deprotonation. The introduction of metal ions was expected to profoundly affect charge transport. However, it was not known whether metal binding would also alter the helical structure as is the case in related pyridinecarboxamide helices, which bind Cu^{II} to form double helicates that are quite distinct from their single helical precursors.^[15] The inner diameter of Q_n helices is narrow, so much so that they are used as capping segments in the design of helical capsules.^[8a,13] Nevertheless, space suitable to fit a small metal ion might be accommodated upon amide deprotonation which would transform each Q unit into a bidentate ligand. Therefore, we endeavored to investigate metal coordination of Cu^{II} by nitro- and ester-terminated Q_{2m+1} oligomers having an odd number of units, that is, an even number of amides.

Mixing Q_3 with $\text{Cu}(\text{OAc})_2$ in $\text{CHCl}_3/\text{MeOH}$ (1:1 vol/vol) led to the instant appearance of a dark green color at room temperature. Binding was found to be strong, and curve fitting of the change of UV/Vis absorbance to a 1:1 binding isotherm yielded a lower estimate for the $K_a > 2.8 \times 10^6 \text{ L mol}^{-1}$ (Supporting Information, Figures S1–S3). When mixing Q_5 with $\text{Cu}(\text{OAc})_2$ under the same conditions, the UV/Vis spectrum stabilized after four days (Figure S4). This slower process may be ascribed to the higher stability of the Q_5 helix and lower solvent exposure of metal binding sites. Other solvent combinations (e.g. CHCl_3 or CH_2Cl_2 and CH_3CN or DMF) led to similar results provided that they could dissolve both the ligand and the $\text{Cu}(\text{II})$ salt. The reduced reaction kinetics were bypassed by increasing the reaction temperature to 60°C . This allowed for the quantitative formation of deprotonated and fully metalated Cu^{II} -loaded $Q_5\cdot 2\text{Cu}$, $Q_7\cdot 3\text{Cu}$ and $Q_9\cdot 4\text{Cu}$ oligomers, as indicated by their clean ESI-MS spectra after aqueous washing to remove excess $\text{Cu}(\text{OAc})_2$ (Figures S7–S9). MS analysis did not detect any trace of multi-stranded helicates. MS also indicated deprotonation of the amides, as confirmed by FT-IR spectroscopy which showed

characteristic changes in the amide I and II regions (Figure S17). Remarkably, the only base present during the reaction is the acetate counterion. We thus infer that the overall neutral complexes that were formed are stable to the small amount of AcOH produced during the reaction. $Q_{2m+1}\cdot m\text{Cu}$ oligomers were nevertheless demetalated and recovered intact by aqueous HCl treatment.

Single crystals of $Q_5\cdot 2\text{Cu}$, $Q_7\cdot 3\text{Cu}$ and $Q_9\cdot 4\text{Cu}$ suitable for X-ray diffraction analysis were obtained by slow evaporation from chloroform/methanol solutions.^[16] The structures all showed that the single helical shape of the quinoline oligoamides was maintained after complexation with Cu^{II} (Figure 2), in sharp contrast with the frequently encountered double stranded helicates.^[4,15] Overlays of the structures of Q_9 and $Q_9\cdot 4\text{Cu}$ confirm minimal changes (a slight decrease in curvature) upon metal complexation (Figure S18). All Cu^{II} coordination spheres are based on the distorted four-coordinate structure shown in Figure 1a. Occasionally, some

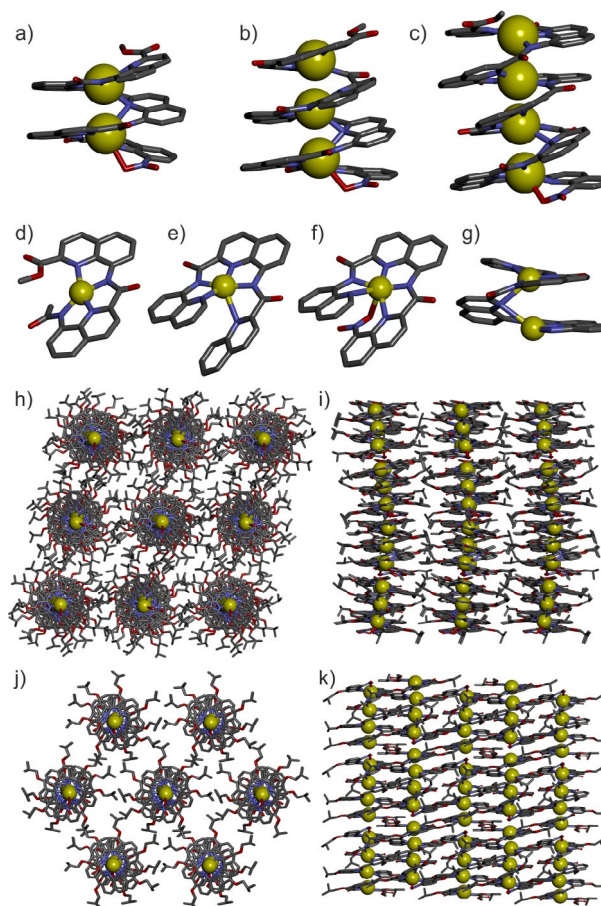


Figure 2. X-ray single-crystal structures of a) $Q_5\cdot 2\text{Cu}$; b) $Q_7\cdot 3\text{Cu}$ and c) $Q_9\cdot 4\text{Cu}$. Hydrogen atoms, isobutyl side chains and included solvent molecules have been removed for clarity. Examples of Cu^{II} centers in $Q_9\cdot 4\text{Cu}$ that are four- (d), five- (e) or six-coordinate (f). See Figure S19 for bond lengths. g) Example of a quinoline ligand that bridges two Cu^{II} centers. Crystal packing of $Q_7\cdot 3\text{Cu}$ viewed along (h) and perpendicular to (i) the foldamers helical axis. Crystal packing of $Q_9\cdot 4\text{Cu}$ viewed along (j) and perpendicular to (k) the foldamers helical axis. Hydrogen atoms and included solvent molecules have been removed for clarity.

endocyclic nitrogen atoms seem to bridge two Cu^{II} centers, and the *N*-terminal nitro group is always involved in coordination with the nearest Cu^{II}, so that distorted five and six coordination are also observed (Figure 2 d–g). The flexible coordination of Cu^{II} thus appears to be a favorable parameter. A few tests were performed with other metals that revealed only weak coordination of Pd^{II} by Q₃ as well as a double stranded (Q₃·Zn)₂ helicate (Figures S13–S16), suggesting that the formation of the Cu^{II} complexes is not general. A thorough screening of other metals was not performed.

Additional experiments shed light on the reaction pathways to form these complexes. Q₇·3Cu was found to lose one Cu^{II} in presence of AcOH. A crystal structure of the resulting Q₇·2Cu was obtained and showed that the *N*-terminal Cu^{II} was missing (Figure S20). Furthermore, when Q₇ was reacted with only 1 equiv of Cu(OAc)₂, a mixture of products was obtained that yielded remarkable co-crystals. The asymmetric unit contained four different complexes: one Q₇·3Cu, two Q₇·2Cu, and one Q₇·Cu (Figure S20). The Cu^{II} occupancy factors were not all 100 %, highlighting that helices may have identical shapes with and without Cu^{II} and take the same position in the lattice. Remarkably, all structures had a fully occupied *C*-terminal Cu^{II}, and the *N*-terminal Cu^{II} was missing in both Q₇·2Cu complexes. In short, the *C*-terminus emerged as a preferred site and the *N*-terminus as a more labile site.

Metalation of Q₁₇ and Q₃₃ was incomplete even after prolonged reactions (75 °C for 2 weeks). We reasoned that full metalation may require a quickly reversible process because random metalation would produce orphan amide groups that can no longer uptake a metal center (Figure 3 a). Indeed, in the absence of a cooperative, zipper-like mechanism, the number of possible pathways and intermediates towards full Cu^{II} loading increases very fast with increasing oligomer length. There are 32 possible intermediates towards Q₉·4Cu, of which 14 need no correction. To produce Q₃₃·16Cu, one can count 3524576 intermediates, of which only 65534 (1.86 %) need no correction (See supporting information), and 5841 are fully loaded but include orphan amides. We thus tested higher temperatures and short reaction times and cleanly obtained Q₁₇·8Cu by heating Q₁₇ with Cu(BF₄)₂ in *N,N*-dimethylformamide at 120 °C for 15 min. Q₃₃·16Cu was obtained similarly, in *N*-methyl-2-pyrrolidone at 150 °C for 20 min. ESI-MS spectra convincingly showed the completion of the reaction (Figure 3 b,c). The counterion used was found to be important. With Cu(OAc)₂ or Cu(OTf)₂, reactions were incomplete and prolonged reactions time at high temperature eventually led to the degradation of the oligomers. The origin of these counterion effects is unclear. Again, the reactions take place in the absence of base. We presume that the HBF₄ by-product is buffered by acid-mediated degradation of the solvent. It may also be that a certain level of acidity is required to reach equilibrium and that this level is not attained with all counterions. In addition, BF₄⁻ anions are known to degrade to produce HF, which might also play a role.

The crystal structures shown in Figure 2 revealed the formation of linear arrays of Cu^{II} centers within the organic helices. The distances between individual Cu^{II} ions inside the

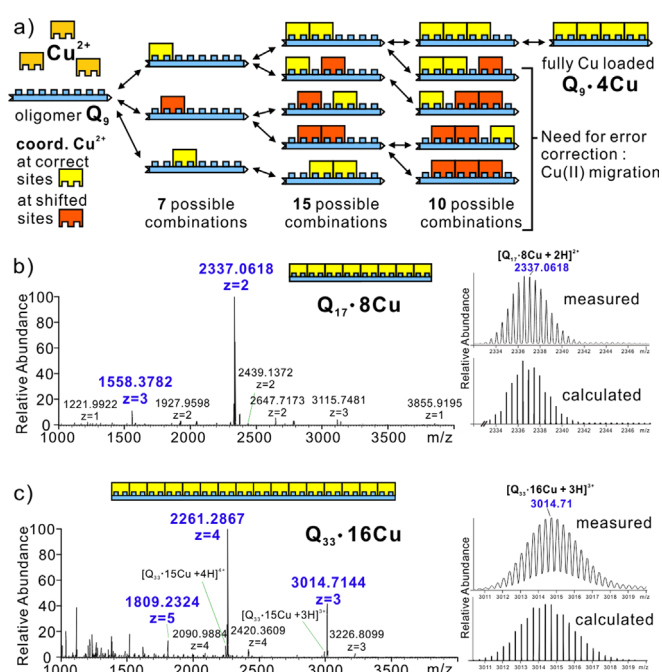


Figure 3. a) Cartoon representing the processes of error-correction towards a fully loaded Q₉·4Cu helix. ESI-MS spectra and isotopic distributions of b) Q₁₇·8Cu and c) Q₃₃·16Cu, the corresponding *m/z* of respective complexes are marked with blue, different charge states were observed in both compounds. Traces of Q₁₇·7Cu and Q₃₃·15Cu, that is, missing one Cu^{II}, are detected, but these may arise from degradation in the gas phase since they are also seen for the shorter complexes in their pure form.

helices are ca. 3 Å, suggesting that only weak or no metal-metal interactions may take place. Indeed metal-metal interactions often require shorter distances (less than ≈2.8 Å for Cu^{II}),^[17] as observed in various Pt and Au-complexes.^[18] Nevertheless, magnetic susceptibility measurements revealed an unanticipated ferromagnetic exchange between the paramagnetic Cu^{II}. The data could be fitted to an isotropic Heisenberg spin Hamiltonian considering spin $S = 1/2$ Cu^{II} centers (Figures S21, S22). The arrangement of the Cu^{II} in the helices suggests a sort of wire. Furthermore, the helices stack in the crystals so as to extend the linear arrays of Cu^{II} throughout the entire crystal (Figure 2 h–k). Within a columnar stack, helices all have the same handedness, and helix-helix contacts are always head-to-tail, resulting in intermolecular Cu–Cu distances in the 4.3–4.5 Å range. This organization along the helix axis prevails even though the in-plane organization of the helices varies: the columns assume a near perfect pseudo-hexagonal close packing and all have the same handedness in the chiral lattice of Q₉·4Cu (Figure 2 j,k) whereas they are both right- and left-handed and adopt an almost square packing in the crystal lattice of Q₇·3Cu (Figure 2 h,i).

We surmised that these materials may behave as strongly anisotropic molecular conductors provided that the alignment of the Cu^{II} ions is conducive to charge transport. Unfortunately, the crystals' robustness was insufficient to directly measure their conductivity using vacuum-deposited electrodes.^[19] We thus turned to probing the conductivity of self-

assembled monolayers (SAMs) of the metalated foldamers forming a metal-organic-metal junction, as performed previously on Q_n oligomers.^[12a] For this purpose, $AsgQ_5$, $AsgQ_9$, and $AsgQ_{17}$ (Figure 4a) were synthesized as analogues of Q_5 , Q_9 , and Q_{17} , respectively (see Supporting Information). In these new compounds, the *N*-terminal 8-nitro group is replaced by an asparagusic amidomethyl group (Asg). $AsgQ_5 \cdot 2Cu$, $AsgQ_9 \cdot 4Cu$ and $AsgQ_{17} \cdot 8Cu$ were generated by carefully optimizing the copper-loading reaction conditions. The absence of degradation of the S–S bond and the identity of each copper-loaded oligomer were confirmed by mass spectrometry (SI for details, Figure S12). SAMs were produced using the asparagusic group as an anchoring site for the gold surface (Figure 4b, see Supporting information). The successful formation of the corresponding monolayers on gold substrates was evidenced by XPS, spectroscopic ellipsometry and polarization-modulated infrared reflection-absorption spectroscopy (PMIRRAS). The thickness of the monolayers obtained for each complex was found to increase with the length of the oligomers as expected for the formation of compact, vertically-aligned helices (Table S2).^[12a,20] Likewise, the PMIRRAS spectra displayed the expected absorption bands corresponding to the metalated foldamers (Figure S23, S24). PMIRRAS signal intensity increases with increasing foldamer length (Figure S23). This can only be possible if the foldamers are oriented perpendicular (i.e. standing vertical or with a constant tilt angle) with respect to the substrate. Finally, the formation of metalated foldamer SAMs was also confirmed by XPS, which clearly showed the

presence of sulfur and copper atoms in the surface composition of the monolayers (Figure S25).

The SAMs are designed to form part of a metal-insulator-metal device with the gold substrate acting as a bottom electrode. The other electrode is formed using a conductive Pt-Ir atomic force microscopy tip (conductive-AFM) which is used to locally probe the conductivity of the SAM at a set force by measuring the current as a function of applied voltage. To circumvent tip variability and contact area, the measurements comparing the conductance of the SAMs were done with the same tip at an applied force of 5.1 nN. Under these conditions, the SAMs exhibited conductances between 2×10^{-8} and 50×10^{-12} S (Figure 4d). Under the same conditions, the conductance of a control non-metalated $AsgQ_9$ SAM was below the detection limit of the instrument.^[21] From this, we deduce that the mechanism of charge transport may be different between the metalated and non-metalated foldamer architectures in spite of their similar size and shape. Cyclic voltammetry experiments performed using the Au substrates modified with the $AsgQ_{2m+1} \cdot mCu$ foldamers (Figure 4c), as well as the cyclic voltammograms of solutions of $Q_{2m+1} \cdot mCu$ foldamers (Figure S26) showed a reduction peak whose area increases with the number of Cu^{II} ions bound inside the foldamers. The peak areas correlate well with the calculated number of electrons necessary for the complete reduction of the copper in the monolayer (Table S3). The molecular surface densities that can be calculated again support an upright orientation of the helices on the surface (Figure S27). Furthermore, no oxidation event was observed over the potential scanned. From this, we deduce that the presence of the Cu^{II} ions is conducive to the transport of electrons via a facile initial reduction step to Cu^I that would produce mixed valence species such as those recently reported for some metallopolymers.^[4c] Some structural variations due to the change in the coordination geometry between the Cu^{II} , which are present in 4-, 5-, or 6-coordinate geometry and Cu^I , which prefers a tetragonal coordination, may be expected. We note that the separation between the forward and return waves increases with increasing number of Cu^{II} ions, and that this is accompanied by a progressive decrease in the reversibility of the redox process. Together, this could be an indication of differences in the rate of the redox process and a reflection of geometrical changes. It remains that, unlike the non-metalated foldamer helices which are hole transporting materials, the Cu^{II} metalated foldamers are geared towards electron transport due to the redox properties of the metal ions.

Comparison of the charge transport properties of the $AsgQ_{2m+1} \cdot mCu$ SAMs reveals that the resistance of the monolayer (R) increases with increasing foldamer length (Figure 4). Linear fitting of a plot of $\ln R$ vs. molecular length for the series yields a value of $0.22 \pm 0.05 \text{ \AA}^{-1}$ for the attenuation factor (see Supporting Information). This value is larger than that determined for the analogous non-metalated foldamers (0.06 \AA^{-1}), which would be consistent with the larger reorganization energy generally associated with electron vs. hole transport.^[22] It is also plausible that, whereas hole transport in the non-metalated foldamers occurs via multiple charge transport pathways, electron transport in

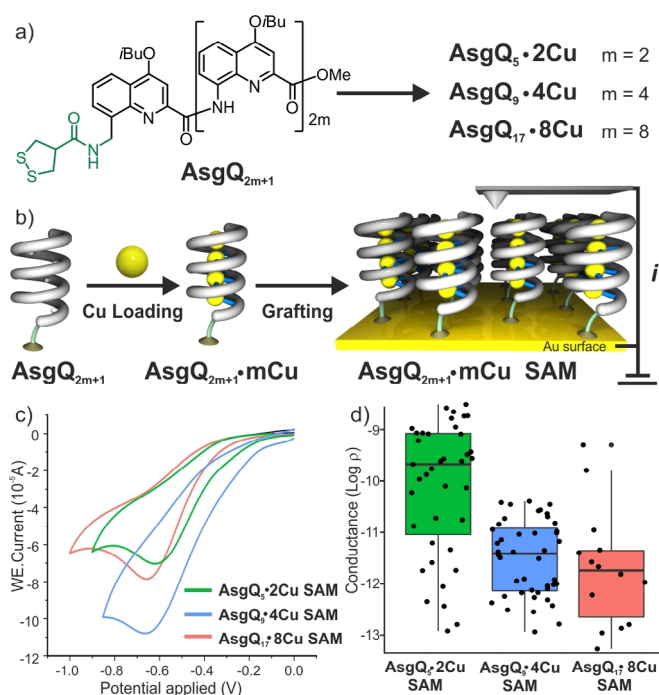


Figure 4. a) Chemical structures of the asparagusic-functionalized metalated foldamers. b) Cartoon representation of the steps to form self-assembled monolayers (SAMs) of Cu-loaded foldamers on a gold substrate; c) Cyclic voltammograms of gold electrodes functionalized with a SAM of the metalated foldamers. d) Statistics of the conductance of SAMs measured using conductive-AFM.

the metalated foldamers can occur solely through the linear array of Cu^{II} ions. The latter is, therefore, more susceptible to disruption due to conformational or localized defects whose probability increases with increasing molecular size.

In conclusion, loading of up to exactly sixteen Cu^{II} ions into quinoline-oligoamide foldamers has been achieved while maintaining their single helical structure. The Cu^{II} centers inside the helices were aligned akin to molecular wires. One dimensional alignment of Cu^{II} also occurred in crystals by stacking of the helices. The effect of copper loading on the conductance through the foldamers was tested by measuring the resistance of self-assembled monolayers using conductive AFM. It was found that copper loading may switch the intrinsic hole transport of the foldamers to electron transport. Switching of the nature of the charge carriers in these foldamers represents a simple way to profoundly alter the electronic properties of the materials. The absence of significant structural alterations upon metalation, as demonstrated by the spontaneous co-crystallization of partially metalated foldamers, may further allow for the construction of multiple molecular *p-n* junctions with relative ease. Progress in this direction is being made and will be reported in due course.

Acknowledgements

This work was supported by the French National Research Agency (grant ANR-18-CE6-0018, FORESEE), the France-Germany International Research Project “Foldamers Structures and Functions” (IRP FoldSFun) and German Research Foundation (DFG) under Germany’s Excellence Strategy—EXC 2089/1-390776260. The China Scholarship Council is gratefully acknowledged for a predoctoral fellowship to J.W. The work benefited from the facilities and expertise of the Biophysical and Structural Chemistry platform at IECB, CNRS UMS3033, INSERM US001, Université de Bordeaux. We thank B. Kauffmann for assistance with crystallographic measurements; F. Rosu for assistance with MS measurements, C. Clérac and M. Rouzières for assistance with magnetic susceptibility measurements, and C. Bao and M. Marchivie for preliminary experiments. Open access funding enabled and organized by Projekt DEAL.

Conflict of interest

The authors declare no conflict of interest.

Keywords: Cu^{II} coordination · electron transport · helix · metallofoldamers · self-assembled monolayers

- [1] a) G. Skorupskii, B. A. Trump, T. W. Kasel, C. M. Brown, C. H. Hendon, M. Dincă, *Nat. Chem.* **2020**, *12*, 131–136; b) J. K. Bera, K. R. Dunbar, *Angew. Chem. Int. Ed.* **2002**, *41*, 4453–4457; *Angew. Chem.* **2002**, *114*, 4633–4637; c) W. J. Cho, Y. Cho, S. K. Min, W. Y. Kim, K. S. Kim, *J. Am. Chem. Soc.* **2011**, *133*, 9364–9369; d) J. Rawson, P. J. Angiolillo, P. R. Frail, I. Goodenough, M. J. Therien, *J. Phys. Chem. B* **2015**, *119*, 7681–7689.

- [2] a) S. Y.-L. Leung, K. M.-C. Wong, V. W.-W. Yam, *Proc. Natl. Acad. Sci. USA* **2016**, *113*, 2845–2850; b) K. M.-C. Wong, V. W.-W. Yam, *Acc. Chem. Res.* **2011**, *44*, 424–434; c) V. W.-W. Yam, K. M.-C. Wong, N. Zhu, *J. Am. Chem. Soc.* **2002**, *124*, 6506–6507; d) Y. Ai, Y. Li, H. L.-K. Fu, A. K.-W. Chan, V. W.-W. Yam, *Chem. Eur. J.* **2019**, *25*, 5251–5258; e) C. Yu, K. M.-C. Wong, K. H.-Y. Chan, V. W.-W. Yam, *Angew. Chem. Int. Ed.* **2005**, *44*, 791–794; *Angew. Chem.* **2005**, *117*, 801–804; f) M. E. Robinson, A. Nazemi, D. J. Lunn, D. W. Hayward, C. E. Boott, M.-S. Hsiao, R. L. Harniman, S. A. Davis, G. R. Whittell, R. M. Richardson, L. De Cola, I. Manners, *ACS Nano* **2017**, *11*, 9162–9175; g) S. Sinn, L. Yang, F. Biedermann, D. Wang, C. Kübel, J. J. L. M. Cornelissen, L. De Cola, *J. Am. Chem. Soc.* **2018**, *140*, 2355–2362; h) A. Aliprandi, M. Mauro, L. De Cola, *Nat. Chem.* **2016**, *8*, 10–15.
- [3] a) M. Albrecht, *Chem. Rev.* **2001**, *101*, 3457–3498; b) C. Piguet, G. Bernardinelli, G. Hopfgartner, *Chem. Rev.* **1997**, *97*, 2005–2062; c) J. M. Lehn, A. Rigault, J. Siegel, J. Harrowfield, B. Chevrier, D. Moras, *Proc. Natl. Acad. Sci. USA* **1987**, *84*, 2565–2569.
- [4] a) J. L. Greenfield, F. J. Rizzuto, I. Goldberga, J. R. Nitschke, *Angew. Chem. Int. Ed.* **2017**, *56*, 7541–7545; *Angew. Chem.* **2017**, *129*, 7649–7653; b) J. L. Greenfield, E. W. Evans, D. Di Nuzzo, M. Di Antonio, R. H. Friend, J. R. Nitschke, *J. Am. Chem. Soc.* **2018**, *140*, 10344–10353; c) J. L. Greenfield, D. Di Nuzzo, E. Evans, S. P. Senanayak, S. Schott, J. T. Deacon, A. Peugeot, W. K. Myers, H. Sirringhaus, R. Friend, J. R. Nitschke, *Adv. Mater.* **2021**, *33*, 2100403.
- [5] a) M. Barboiu, A.-M. Stadler, J.-M. Lehn, *Angew. Chem. Int. Ed.* **2016**, *55*, 4130–4154; *Angew. Chem.* **2016**, *128*, 4200–4225; b) M. Barboiu, J.-M. Lehn, *Proc. Natl. Acad. Sci. USA* **2002**, *99*, 5201–5206; c) A.-M. Stadler, N. Kyritsakas, J.-M. Lehn, *Chem. Commun.* **2004**, 2024–2025; d) A.-M. Stadler, J.-M. P. Lehn, *J. Am. Chem. Soc.* **2014**, *136*, 3400–3409; e) B. Hasenknopf, J.-M. Lehn, N. Boumediene, E. Leize, A. Van Dorselaer, *Angew. Chem. Int. Ed.* **1998**, *37*, 3265–3268; *Angew. Chem.* **1998**, *110*, 3458–3460.
- [6] a) K. Tanaka, A. Tengeiji, T. Kato, N. Toyama, M. Shionoya, *Science* **2003**, *299*, 1212–1213; b) G. H. Clever, K. Polborn, T. Carell, *Angew. Chem. Int. Ed.* **2005**, *44*, 7204–7208; *Angew. Chem.* **2005**, *117*, 7370–7374; c) G. H. Clever, T. Carell, *Angew. Chem. Int. Ed.* **2007**, *46*, 250–253; *Angew. Chem.* **2007**, *119*, 254–257; d) Y. Takezawa, M. Shionoya, *Acc. Chem. Res.* **2012**, *45*, 2066–2076; e) I. Sinha, C. Fonseca Guerra, J. Müller, *Angew. Chem. Int. Ed.* **2015**, *54*, 3603–3606; *Angew. Chem.* **2015**, *127*, 3674–3677; f) B. Jash, J. Müller, *Angew. Chem. Int. Ed.* **2018**, *57*, 9524–9527; *Angew. Chem.* **2018**, *130*, 9668–9671; g) J. Müller, *Coord. Chem. Rev.* **2019**, *393*, 37–47; h) T. Funai, C. Tagawa, O. Nakagawa, S.-i. Wada, A. Ono, H. Urata, *Chem. Commun.* **2020**, 56, 12025–12028.
- [7] a) W. Tress, K. Leo, M. Riede, *Adv. Funct. Mater.* **2011**, *21*, 2140–2149; b) D. Poplavskyy, J. Nelson, *J. Appl. Phys.* **2003**, *93*, 341–346; c) L. Zang, Y. Che, J. S. Moore, *Acc. Chem. Res.* **2008**, *41*, 1596–1608; d) Y. Shirota, H. Kageyama, *Chem. Rev.* **2007**, *107*, 953–1010; e) V. Coropceanu, J. Cornil, D. A. da Silva Filho, Y. Olivier, R. Silbey, J.-L. Brédas, *Chem. Rev.* **2007**, *107*, 926–952.
- [8] a) Y. Ferrand, I. Huc, *Acc. Chem. Res.* **2018**, *51*, 970–977; b) X. Hu, S. J. Dawson, P. K. Mandal, X. de Hatten, B. Baptiste, I. Huc, *Chem. Sci.* **2017**, *8*, 3741–3749; c) S. De, B. Chi, T. Granier, T. Qi, V. Maurizot, I. Huc, *Nat. Chem.* **2018**, *10*, 51–57; d) K. Ziach, C. Chollet, V. Parissi, P. Prabhakaran, M. Marchivie, V. Corvaglia, P. P. Bose, K. Laxmi-Reddy, F. Godde, J.-M. Schmitter, S. Chaignepain, P. Pourquier, I. Huc, *Nat. Chem.* **2018**, *10*, 511–518.
- [9] *Metallofoldamers* (Eds.: G. Maayan, M. Albrecht), Wiley-VCH, Weinheim, **2013**.

- [10] a) T. Qi, V. Maurizot, H. Noguchi, T. Charoenraks, B. Kauffmann, M. Takafuji, H. Ihara, I. Huc, *Chem. Commun.* **2012**, 48, 6337–6339; b) H. Jiang, J.-M. Léger, I. Huc, *J. Am. Chem. Soc.* **2003**, 125, 3448–3449.
- [11] a) T. Qi, T. Deschrijver, I. Huc, *Nat. Protoc.* **2013**, 8, 693; b) X. Li, T. Qi, K. Srinivas, S. Massip, V. Maurizot, I. Huc, *Org. Lett.* **2016**, 18, 1044–1047.
- [12] a) A. Méndez-Ardoy, N. Markandeya, X. Li, Y.-T. Tsai, G. Pecastaings, T. Buffeteau, V. Maurizot, L. Muccioli, F. Castet, I. Huc, D. M. Bassani, *Chem. Sci.* **2017**, 8, 7251–7257; b) X. Li, N. Markandeya, G. Jonusauskas, N. D. McClenaghan, V. Maurizot, S. A. Denisov, I. Huc, *J. Am. Chem. Soc.* **2016**, 138, 13568–13578; c) M. Wolffs, N. Delsuc, D. Veldman, N. V. Anh, R. M. Williams, S. C. J. Meskers, R. A. J. Janssen, I. Huc, A. P. H. J. Schenning, *J. Am. Chem. Soc.* **2009**, 131, 4819–4829.
- [13] P. Mateus, A. Jacquet, A. Méndez-Ardoy, A. Bouloy, B. Kauffmann, G. Pecastaings, T. Buffeteau, Y. Ferrand, D. M. Bassani, I. Huc, *Chem. Sci.* **2021**, 12, 3743–3750.
- [14] G. V. Dubacheva, M. Devynck, G. Raffy, L. Hirsch, A. Del Guerso, D. M. Bassani, *Small* **2014**, 10, 454–461.
- [15] V. Maurizot, G. Linti, I. Huc, *Chem. Commun.* **2004**, 924–925.
- [16] Deposition Numbers 2074374 (for $(Q_3Zn)_2$), 2074375 (for Q_5-2Cu), 2074376 (for $Q_7-3Cu + 2(Q_7-2Cu) + Q_7-Cu$), 2074377 (for Q_7-2Cu), 2074378 (for Q_7-3Cu), 2074379 (for Q_9-4Cu) contain the supplementary crystallographic data for this paper. These data are provided free of charge by the joint Cambridge Crystallographic Data Centre and Fachinformationszentrum Karlsruhe Access Structures service www.ccdc.cam.ac.uk/structures.
- [17] a) C.-M. Che, S.-W. Lai, *Coord. Chem. Rev.* **2005**, 249, 1296–1309; b) K. M. C. Wong, V. K. M. Au, V. W. W. Yam in *Comprehensive Inorganic Chemistry II*, 2nd ed. (Eds.: J. Reedijk, K. Poepelmeier), Elsevier, Amsterdam, **2013**, pp. 59–130; c) P. Pyykkö, *Chem. Rev.* **1997**, 97, 597–636; d) A. Bondi, *J. Phys. Chem.* **1964**, 68, 441–451.
- [18] a) M.-Y. Leung, S. Y.-L. Leung, K.-C. Yim, A. K.-W. Chan, M. Ng, V. W.-W. Yam, *J. Am. Chem. Soc.* **2019**, 141, 19466–19478; b) Y.-S. Wong, M. Ng, M. C.-L. Yeung, V. W.-W. Yam, *J. Am. Chem. Soc.* **2021**, 143, 973–982; c) M. P. Laurent, J. C. Tewksbury, M.-B. Krogh-Jespersen, H. Patterson, *Inorg. Chem.* **1980**, 19, 1656–1662; d) Z. Assefa, B. G. McBurnett, R. J. Staples, J. P. Fackler, B. Assmann, K. Angermaier, H. Schmidbaur, *Inorg. Chem.* **1995**, 34, 75–83; e) J. K.-L. Poon, Z. Chen, S. Y.-L. Leung, M.-Y. Leung, V. W.-W. Yam, *Proc. Natl. Acad. Sci. USA* **2021**, 118, e2022829118.
- [19] a) C. Reese, Z. Bao, *Adv. Mater.* **2007**, 19, 4535–4538; b) H. Jiang, W. Hu, *Angew. Chem. Int. Ed.* **2020**, 59, 1408–1428; *Angew. Chem.* **2020**, 132, 1424–1445.
- [20] a) J. C. Love, L. A. Estroff, J. K. Kriebel, R. G. Nuzzo, G. M. Whitesides, *Chem. Rev.* **2005**, 105, 1103–1170; b) M. A. Ramin, G. Le Bourdon, N. Daugey, B. Bennetau, L. Vellutini, T. Buffeteau, *Langmuir* **2011**, 27, 6076–6084.
- [21] We consider this single reference value to be insufficient to formulate a general claim that Cu^{II} loading enhances charge transport in Q_n oligomers. A conductance of 14×10^{-12} S was obtained for $AsgQ_9$ SAMs at a higher 20.4 nN applied tip force. This conductance value is similar to that recently reported for an analogous foldamer capsule under similar conditions (Ref. [13]) but somewhat lower than previously measured for more compact foldamer SAMs incorporating a single thiol anchoring point (Ref [12a]).
- [22] a) B. C. Lin, C. P. Cheng, Z. P. M. Lao, *J. Phys. Chem. A* **2003**, 107, 5241–5251; b) H.-Y. Chen, I. Chao, *Chem. Phys. Lett.* **2005**, 401, 539–545; c) Z. Shuai, H. Geng, W. Xu, Y. Liao, J.-M. André, *Chem. Soc. Rev.* **2014**, 43, 2662–2679; d) X.-D. Tang, Y. Liao, H. Geng, Z.-G. Shuai, *J. Mater. Chem.* **2012**, 22, 18181–18191.

Manuscript received: April 6, 2021

Revised manuscript received: May 12, 2021

Accepted manuscript online: May 20, 2021

Version of record online: ■■■■■■

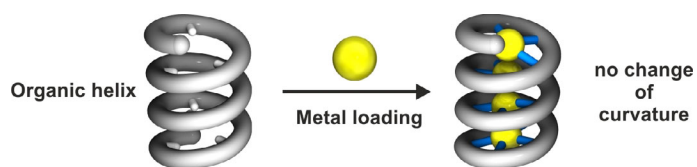
Communications



Metallofoldamers

J. Wang, B. Wicher, A. Méndez-Ardoy,
X. Li, G. Pecastaings, T. Buffeteau,
D. M. Bassani, V. Maurizot,
I. Huc* ————— ■■■-■■■

Loading Linear Arrays of Cu^{II} Inside
Aromatic Amide Helices



Very stable helices of oligoamides uptake Cu^{II} ions in their cavity through deprotonation with minimal alteration of their shape, unlike most metallo-organic structures which generally differ from

their organic precursors. The outcome is the formation of intramolecular linear arrays of up to 16 Cu^{II} centers, forming a molecular mimic of a metal wire completely surrounded by an organic sheath.